Chinese Chemical Letters 33 (2022) 930–934

Contents lists available at ScienceDirect

Chinese Chemical Letters

journal homepage: www.elsevier.com/locate/cclet

Micrometer-sized NiOOH hierarchical spheres for enhanced degradation of sulfadiazine *via* synergistic adsorption and catalytic oxidation in peroxymonosulfate system

Cong Lyu[a,b], Lu Zhang[a,b], Dan He[a,b], Boyuan Su[c], Ying Lyu[a,b,*]

[a] Key Lab of Groundwater Resources and Environment, Ministry of Education, Jilin University, Changchun 130026, China
[b] Jilin Provincial Key Laboratory of Water Resources and Environment, Jilin University, Changchun 130026, China
[c] Department of Chemistry and Environmental Science, New Jersey Institute of Technology, Newark, NJ 07102, United States

ARTICLE INFO

Article history:
Received 3 May 2021
Revised 14 June 2021
Accepted 5 July 2021
Available online 14 July 2021

Keywords:
Nickel oxyhydroxide
Peroxymonosulfate
Sulfate radical
Singlet oxygen
Sulfadiazine

ABSTRACT

As an antibiotic, sulfadiazine has posed a serious threat to humans and ecosystems due to its chronic toxicity. The advanced oxidation processes (AOPs) *via* heterogeneous catalytic activation of peroxymonosulfate (PMS) have significant potential for the degradation of antibiotics. However, there are multiple restrictions including non-specifically binding to target contaminants, which would deplete oxidation capacity, and lacking energy effectiveness due to inefficient utilization of reactive oxygen species (ROS). To overcome these obstacles, we adopted the "bait-hook & destroy" strategy in this study. Herein, we synthesized a novel micrometer-sized NiOOH hierarchical spheres assembled from nanosheets, which have relatively large specific surface areas and yield specified cavities to "bait-hook" sulfadiazine and PMS onto the surface cavities. This process was further conductive to effective generation of ROS and subsequently "destruction" of sulfadiazine with elevated mass transformation rate. 20.4% of sulfadiazine can adsorb to NiOOH surface in less than 30 min (0.0051 min^{-1}), and then sulfadiazine was completely degraded in 90 min intervals in the NiOOH/PMS system. The degradation rate constant (k = 0.0537 min^{-1}) was about 5.3, 2.5 and 2.2 times higher than that in Ni_2O_3/PMS, NiO/PMS and $Ni(OH)_2$/PMS system, respectively. This was ascribed to the synergistic catalytic oxidation and adsorption process occurred on the surface of NiOOH. Appreciably, there were both non-radicals ($^1O_2$) and radicals ($O_2^{\bullet-}$ and $SO_4^{\bullet-}$) involved in the NiOOH/PMS system, and $^1O_2$ was distinguished as the dominated ROS for degradation of sulfadiazine. This study provides a novel strategy *via* synergistic adsorption and catalytic oxidation, and indicates that the micrometer-sized NiOOH hierarchical sphere as heterogeneous catalyst is an attractive candidate for potential application of the SR-AOPs technology in water treatment.

Sulfadiazine has attracted wide-spread attention since it is extensively applied as an antibiotic pharmaceutical in both veterinary and human medicine, and it can pose serious threats to human well-being and ecosystems [1,2]. Conventional wastewater disposal systems, which typically based on the biological treating method, perform poorly on sulfadiazine removal due to the high toxicity and poor biodegradability of sulfadiazine [3,4]. As reported, sulfate radical ($SO_4^{\bullet-}$) based advanced oxidation processes (SR-AOPs) could be regarded as competent, environmentally friendly, and reliable assistants to completely remove antibiotic pharmaceuticals [5,6]. As such, $SO_4^{\bullet-}$ is usually obtained by activating peroxymonosulfate (PMS) [7] and persulfate (PS) [8] in association with ultraviolet [9], heating [10], cavitation [11], microwaves [12], transition metals [3], and so on. Due to the asymmetric molecular structure and low activation energy, PMS is relatively easier to be activated than PS [13]. While compared with other energy-based activation methods, transition metals activation is a much simpler attribute to its lower energy consumption and cost-effectiveness [14,15].

Cobalt ion (Co^{2+}) has proven to be the best PMS activator [16]. Unfortunately, the rather low recycling rate of catalysts in the homogeneous systems significantly inhibits further development [17,18], and the leaching Co^{2+} can hold critical cytotoxicity to ecosystem and human health [19]. Thus, environmental-friendly heterogeneous catalysts, such as Ni, Fe or Mn-based materials in PMS activation, have the potential to overcome limitations [20-22]. Particularly, nickel (Ni) is considered as one of the most abundant elements on the earth and is of less toxic than other transitional

* Corresponding author.
E-mail address: yinglyu@jlu.edu.cn (Y. Lyu).

https://doi.org/10.1016/j.cclet.2021.07.012
1001-8417/

metals [23]. Ni-based heterogeneous catalysts, such as NiO [24], $Ni(OH)_2$ [25] and Ni_2O_3 [26], were proven to be efficient PMS activators in the SR-AOPs system. The redox cycle of Ni^{2+}/Ni^{3+} can improve the highly efficient PMS activation and enhance the generation of reactive oxygen species (ROSs) Eqs. 1 and 2.

$$\equiv Ni^{3+} + HSO_5^- \rightarrow \equiv Ni^{2+} + SO_5^{\bullet -} + H^+ \quad (1)$$

$$\equiv Ni^{2+} + HSO_5^- \rightarrow \equiv Ni^{3+} + SO_4^{\bullet -} + OH^- \quad (2)$$

However, in the PMS system, target contaminants cannot be effectively removed by ROSs since only a small fraction of ROSs can end up reacting the target contaminants, while the partial of ROSs are either scavenged by background constituents (*e.g.*, NOM, bicarbonate, Cl^- *etc.*) or undergoing fast self-decay [27]. Several researchers emphasized the "bait-hook & destroy" strategy to ameliorate the ROS production and utilization, as well as the degradation effect of contaminants [28,29]. Compared with the exclusive adsorption strategy and SR-AOP strategy, the "bait-hook & destroy" strategy could not only pre-concentrate target contaminants from the solution, and further decompose them *in-situ*, into low- or non-toxic products [30]. The ideal catalyst can be used as the "hook" in providing elevated adsorption affinity for sulfadiazine and conduct sulfadiazine accessible to ROSs generation sites, which would facilitate concerning contaminants onto catalyst surface for the following degradation [31,32]. Furthermore, adequate catalytic activity for the PMS activation process could also help to form ROSs. And subsequently ROSs can efficiently react with the adsorbed contaminants, which are referred to as the "destroy" process and elevate the mass transformation rate of catalyst on its surface. Therefore, there is urgently demanded in developing a novel Ni-based heterogeneous catalyst, which can utilize the "bait-hook & destroy" strategy to degrade sulfadiazine.

Nickel oxyhydroxide (NiOOH) has drawn extensive attention as a revolutionary catalyst, and exhibits prominent adsorption capacity owing to its magnificent characteristics, including notable adsorption capacity, robust electron transfer rate, and sufficient catalytic active sites [33]. It is worth noting that the redox potential of Ni^{3+}/Ni^{2+} (2.0 V) is higher than PMS (1.8 V) [34], indicating that NiOOH has substantial application potential for PMS activation. However, since the surface of NiOOH is hydrophilic, it has a poor affinity for sulfadiazine. To offset its limitation, we attempted to regulate the size, morphology, and microstructures of NiOOH through chemical precipitation processes [35].

In this study, we applied micrometer-sized NiOOH hierarchical spheres prepared *via* chemical precipitation method [33], and it exhibits remarkable adsorption capacity and catalytic oxidation competence in the PMS system. Micrometer-sized NiOOH hierarchical spheres, which assembled from nanosheets, have large specific surface areas and produce specified cavities to adsorb sulfadiazine and PMS onto the NiOOH surface. This process was further conducive to the effective generation of ROS and subsequently degrading process of sulfadiazine. Furthermore, the underlying mechanism of sulfadiazine degradation was investigated by quenching tests, X-ray photoelectron spectroscopy (XPS) and electron spin-resonance spectroscopy (ESR) analysis.

The main reagents, preparation, and characterization of NiOOH, experimental procedure, and analysis methods are exhibited in the Supporting information. The X-ray diffraction (XRD) patterns (Fig. 1a) showed that there are diffraction peaks at 12.6°, 25.5°, 37.6°, 42.7°, 51.0° and 66.0°, corresponding to the (003), (006), (102), (105), (108) and (110) (PDF #06-0075), respectively. The peaks of impurities were not detected in XRD patterns, indicating that NiOOH microparticles synthesized through chemical precipitation processes are of stable crystal formation. Energy dispersive spectrometer (EDS) image (Fig. S1 in Supporting information) exhibited that the quantity ratio of nickel atoms to oxygen atoms was about 1:2, which is unanimous about the atomic quantity ratio of nickel and oxygen in NiOOH. Fig. 1b reveals the constituent nanosheets and surface morphology of the synthesized NiOOH. It has the morphology of micrometer-sized hierarchical spheres assembled from nanosheets, which endows it a larger specific surface area and thereby provides abundant catalytic active sites [33]. NiOOH has a rather larger specific surface area (35.2 m^2/g) compared to other nickel-based catalysts (nanosized $Ni(OH)_2$, 20.9 m^2/g) (Table S1 in Supporting information), hence enhancing the surface contact among the sulfadiazine, PMS and NiOOH, exposing more catalytic sites, and increasing the utilization of ROS [36]. According to the FTIR spectrum (Fig. 1c), the strong and sharp band centered at 567 cm^{-1} represents the movement of hydrogen-bonded linkages Ni-O-H and to the stretching vibration of Ni^{3+}-O. The board band at 3450 cm^{-1}, which is congruous with the characteristic of the hydroxyl group, indicates the presence of hydroxyl (-OH) [37-39]. Thus, we could confirm that NiOOH was purely synthesized in this study. The synthesized NiOOH samples displayed type IV isotherms, which reveals that it has a representative mesoporous structure [40]. As show in Fig. 1d, the maximum observation pore size of NiOOH catalyst distribution is 22.35 nm. In addition, the average pore size (15.8 nm) and total pore volume (0.14 cm^3/g) of the NiOOH were calculated by Barret-Joyner-Halenda (BJH) simulation (Table S1). It is worth noting that the absorption of sulfadiazine is available, since the pore diameters of NiOOH are significantly larger than sulfadiazine (14.9 × 6.31 × 4.86 Å) [41].

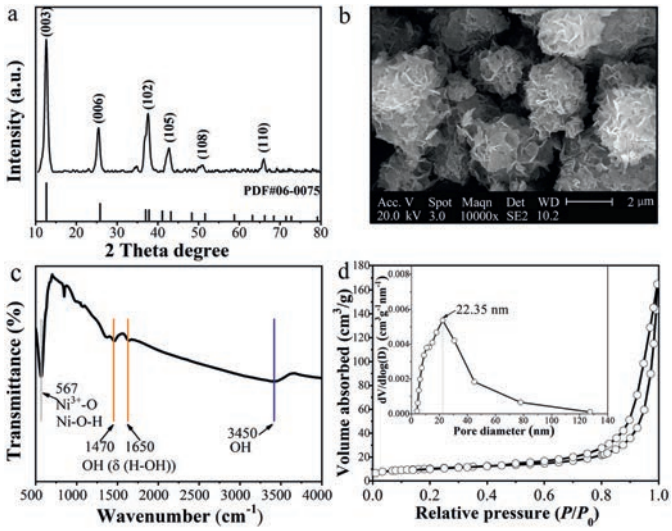

Fig. 1. Characterizations of NiOOH: (a) XRD spectrum, (b) SEM image, (c) FT-IR spectrum and (d) N_2 adsorption-desorption curves and pore size distribution of NiOOH.

The adsorption of NiOOH on P MS activation for sulfadiazine degradation was evaluated. It can be seen from Fig. 2a that 23.2% of sulfadiazine can be adsorbed on the NiOOH surface and the calculated saturated adsorption capacity (q_e) of sulfadiazine is 11.6 mg/g. 46.3% of sulfadiazine was removed within 90 min, implying that the catalytic oxidation process occurred for sulfadiazine degradation. Notably, the synergistic adsorption and catalytic oxidation removal rate of sulfadiazine (0.0537 min^{-1}) was 2.65 times greater than the total contribution of adsorption and catalytic oxidation (0.0051 + 0.0096 = 0.0147 min^{-1}) (Fig. 2b). The removal rate of sulfadiazine was increased significantly may attribute to the enrichment of sulfadiazine onto the surface of NiOOH *via* the hydrogen bonding (OH···N), and the effective utilization of ROS. As illustrated in Fig. 2c, in 90 min reaction, sulfadiazine was completely degraded in 90 min intervals in the NiOOH/PMS system, neverthe-

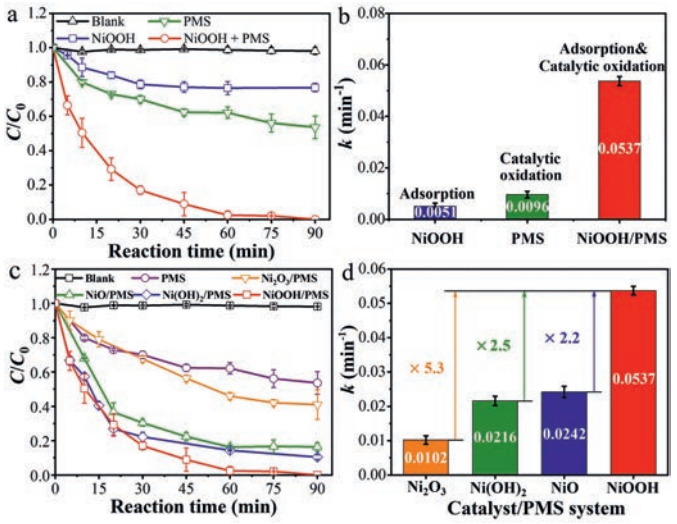

Fig. 2. Adsorption and catalytic oxidation of different catalysts towards sulfadiazine. Degradation kinetics (a, c) and reaction rate (b, d) constants of sulfadiazine in different catalytic PMS system. Conditions: [sulfadiazine] = 10 mg/L, [PMS] = 0.2 mmol/L, [catalysts] = 0.2 g/L, pH 7, T = 20 °C.

less, only 59%, 84% and 90% degradation were accomplished in the Ni_2O_3/PMS, $Ni(OH)_2$/PMS and NiO/PMS system, respectively. Furthermore, based on the first-order kinetic model, the degradation efficiency of sulfadiazine (0.0537 min^{-1}) in NiOOH/PMS system was about 5.3, 2.5 and 2.2 times higher than that in Ni_2O_3/PMS, NiO/PMS and $Ni(OH)_2$/PMS system (Fig. 2d). Conclusively, NiOOH exhibited much higher catalytic performance for PMS activation than Ni_2O_3, NiO and $Ni(OH)_2$.

In particular, the fitting correlation coefficient of the quasi-first-order kinetic model is higher (R^2 = 0.9833) than quasi-second-order kinetic model (R^2 = 0.9463), indicating that sulfadiazine was adsorbed onto NiOOH *via* the formation of hydrogen bonds (O−H···N) between the amino group (−NH) of sulfadiazine and hydroxy (−OH) of NiOOH [42,43] (Fig. S2 in Supporting information). The effects of operation parameters like temperature, sulfadiazine doses, PMS doses, NiOOH doses, background constituents (*e.g.*, NOM, bicarbonate, Cl^- *etc.*), and the rate constant (k) of the NiOOH/PMS system were shown in Figs. S3-S5 (Supporting information). TOC removal rate during the sulfadiazine degradation in NiOOH/PMS system was investigated in Fig. S6 (supporting information). After 90 min, with the complete degradation of sulfadiazine, the removal ratio of TOC increased up to 59.9%, suggesting that more degradation intermediates of sulfadiazine were further completely degraded. More importantly, NiOOH has good stability and recyclability under the initial condition of neutral pH, and it is an attractive candidate for PMS activation to degrade antibiotic pharmaceuticals, as a result of Fig. S7 (Supporting information).

The XPS spectra of NiOOH before and after the catalytic reaction were favorable to evaluate the role of the O and Ni species in the PMS activation. The peaks of Ni 2p at 855.4 eV and 856.4 eV were represented Ni(II) and Ni(III), respectively [44] (Fig. 3a). After the reaction, the peak area of Ni(III) peak was decreased from 100.0% to 33.9%, while the peak area of Ni(II) peak was increased from 0% to 66.1%, which indicates that Ni(III) was reduced to Ni(II) during the reaction. The existence of Ni(II) on the highly hydroxylated surface of NiOOH is beneficial to the formation of Ni-OH^+ active species, which can enhance PMS activation to produce $SO_4^{\bullet-}$ and other active oxygen species for sulfadiazine degradation. The peaks of O 1s performed at 533.0 eV, 531.3 eV and 529.1 eV (Fig. 3b), which was ascribed to adsorbed oxygen (O_{abs}), hydroxyl oxygen (Ni-OH) and lattice oxygen (Ni-O), respectively. Specifically, the Ni-O content hardly changed after the reaction, whereas the amounts of Ni-OH increased and the amounts of O_{abs} decreased. It was ascribed to the formation more of Ni-OH^+ species on the NiOOH surface (Table S2 in Supporting Information). Taken together, cycling of Ni valance and formation of Ni-OH^+ provided a good explanation for the mechanism of PMS activation *via* NiOOH.

To determine the role of various ROS in sulfadiazine degradation, FFA, EtOH, TBA and *p*-BQ were used as quenchers of $^1O_2$, $SO_4^{\bullet-}$, $^{\bullet}OH$ and $O_2^{\bullet-}$ to perform the quenching reactions [45], respectively (Fig. 3c). Detailed discussion is presented in the supplement information. In order to further identify the various ROS in the NiOOH/PMS system and verify the results of the quenching experiment discussion, DMPO and TEMP were added to conduct the characterization of ESR. Under the secondary redox condition, DMPO can react with ROS to generate adducts, such as DMPO-$^{\bullet}OH$, DMPO-$SO_4^{\bullet-}$ and DMPO-$O_2^{\bullet-}$, while TEMP can react with $^1O_2$ to generate TEMP-$^1O_2$, which resulted in the detection of characteristic peaks on the ESR spectrum [46]. The strong ESR signal shown in the Fig. 3d was DMPO-$^{\bullet}OH$, which with a peak-to-height ratio of 1:2:2:1, simultaneously, the low peaks were most likely to be DMPO-$SO_4^{\bullet-}$ [47]. Apparently, four characteristic peaks were conducted in Fig. 3e, which are most likely to be DMPO-$O_2^{\bullet-}$ [48]. In addition, Fig. 3f illustrated a typical TEMP-$^1O_2$ signal, which performed as a three-equal-intensity-line in ESR pattern with the relative intensity of 1:1:1 [49]. Consistent with the quenching experiment results, there were both non-radicals (such as $^1O_2$) and radicals ($O_2^{\bullet-}$ and $SO_4^{\bullet-}$) occurred in the NiOOH/PMS system, and $^1O_2$ was distinguished as the dominated ROS [50].

The degradation intermediates were detected through LC-MS-MS, and seventeen degradation intermediates were observed, and the details are exhibited in Fig. S8 and Table S4 (Supporting information). Practicable pathways of the degrading reaction were proposed in Fig. S9 (Supporting Information). In the first route, the hydrogen-nitrogen bonds of sulfadiazine were stroked by ROS ($SO_4^{\bullet-}$, $O_2^{\bullet-}$ and $^1O_2$) and hydroxylation reaction happened, resulting in the creation of intermediate compound **17** with *m/z* 283.52 [51]. In the second route, the Nitrogen-Carbon bond of sulfadiazine was stroked, and then form the intermediate compound **15** with *m/z* 235.37. Subsequently, the generation of intermediate compound **12** with *m/z* 199.00 derived from the cleavage of pyrimidine ring, owing to the instability of nitrogen-carbon bonds [52]. In the third pathway, sulfadiazine experiences sulfur dioxide extrusion to yield intermediate compound **11** with *m/z* 186.66. In the fourth route, the cleavage of the neighboring sulfur-nitrogen bonds *via* ROS result in intermediate compound **8** with *m/z* 173.21, and intermediate **8** may hydroxylate instantly and converted to intermediate **5** with *m/z* 111.83 [51]. Every single determined intermediate may further degrade in the following reaction by ROS, bring about the generation of aliphatic carboxylic acid, and eventually degrade to CO_2 and H_2O [53].

In accordance with preceding experimental findings, the synergism between the catalytic oxidation and the adsorption process on the NiOOH surface could depict in Fig. 4. Micrometer-sized NiOOH hierarchical spheres used nanosheets as components, which contribute to the extensive specific surface area, and this feature can improve the adsorption of sulfadiazine and PMS. The NiOOH can be used as the "hook" in providing elevated adsorption affinity for sulfadiazine and conducting sulfadiazine accessible to ROSs generation site, which would facilitate concerning sulfadiazine onto NiOOH surface for the following degradation. Furthermore, the hydrogen bonding (O···N) formed between the surface hydroxyl group of NiOOH and the amide group of sulfadiazine could accelerate the absorption of sulfadiazine Fig. 4b). Referring to XPS characterization, quenching experiment, and ESR characterization, NiOOH could concisely activate PMS through non-radical and free radical pathways, as shown in Fig. 4c. The ROS produced *via*

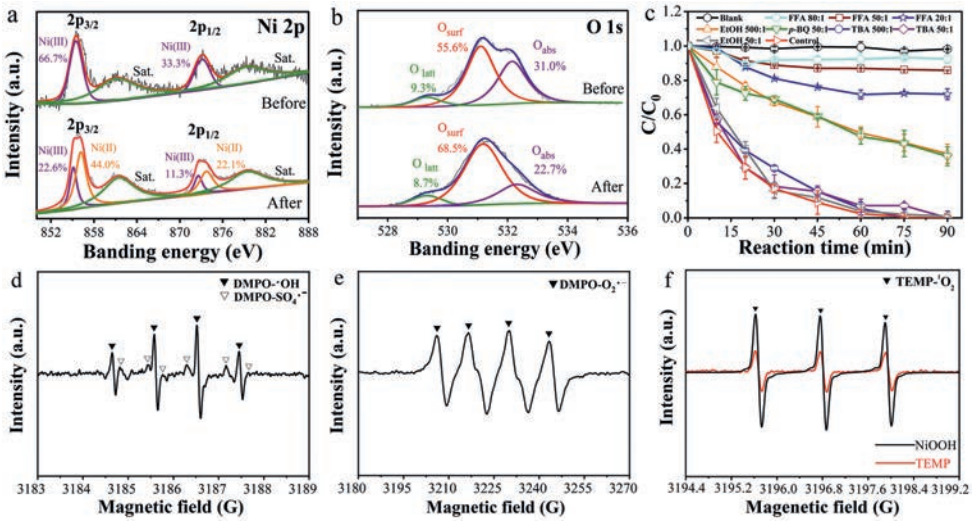

Fig. 3. High-resolution XPS spectra of (a) Ni 2p and (b) O 1s before and after the catalytic oxidation process. Quenching tests and ESR spectrum in the "NiOOH activated PMS" system: (c) The effect of different quenchers on the sulfadiazine degradation in the NiOOH/PMS system and the ESR spectrum of (d) $SO_4^{\bullet-}$ and $^{\bullet}OH$, (e) $O_2^{\bullet-}$ and (f) $^1O_2$ in the NiOOH/PMS system. Conditions: [sulfadiazine] = 10 mg/L, [PMS] = 0.2 mmol/L, [NiOOH] = 0.2 g/L, [FFA] = [*p*-BQ] = 10 mmol/L, [TBA] = [EtOH] = 100 mmol/L, pH 7, T = 20 °C.

Fig. 4. The mechanism of sulfadiazine degradation in the NiOOH/PMS system. The "bait-hook & destroy" strategy (a) combined with sulfadiazine adsorption (b) and ROS generation (c) for sulfadiazine degradation.

PMS activation by NiOOH, including $SO_4^{\bullet-}$, $O_2^{\bullet-}$ and $^1O_2$, can be effectively utilized to degrade sulfadiazine (Eqs. 1-12).

$$\equiv Ni^{2+} + H_2O \rightarrow \equiv Ni - OH^+ + H^+ \quad (3)$$

$$\equiv Ni - OH^+ + HSO_5^- \rightarrow \equiv Ni - O + SO_4^{\bullet-} + H_2O \quad (4)$$

$$\equiv Ni{-}O^+ + 2H^+ \rightarrow \equiv Ni^{3+} + H_2O \quad (5)$$

$$HSO_5^- + OH^- \rightarrow H_2O + SO_5^{2-} \quad (6)$$

$$SO_5^{2-} + H_2O \rightarrow SO_4^{2-} + H_2O_2 \quad (7)$$

$$H_2O_2 + {}^{\bullet}OH \rightarrow HO_2^{\bullet} + H_2O \quad (8)$$

$$HO_2^{\bullet} \rightarrow H^+ + O_2^{\bullet-} \quad (9)$$

$$O_2^{\bullet-} + {}^{\bullet}OH \rightarrow OH^- + {}^1O_2 \quad (10)$$

$$O_2^{\bullet-} + 2H_2O \rightarrow H_2O_2 + {}^1O_2 + 2OH^- \quad (11)$$

$$HSO_5^- + SO_5^{2-} \rightarrow HSO_4^- + SO_4^{2-} + {}^1O_2 \quad (12)$$

Micrometer-sized hierarchical spheres assembled from nanosheets provide abundant catalytic active sites in enriching sulfadiazine and PMS, and then ROS can be effectively utilized to accelerate the sulfadiazine degrading process in the NiOOH/PMS system. Therefore, sulfadiazine might be effectively degraded in the NiOOH/PMS system through the synergism between the catalytic oxidation and the adsorption process.

In summary, a micrometer-sized NiOOH hierarchical sphere assembled from nanosheets with a large specific surface area has been successfully synthesized *via* the chemical precipitation method. Herein, we adopted the "bait-hook & destroy" strategy to enrich sulfadiazine and PMS onto the surface of NiOOH, and then ROS can be effectively generated and utilized for sulfadiazine degradation. Particularly, both radicals and non-radicals occurred in the PMS activation, in which $^1O_2$ might play an important role in sulfadiazine degradation. Overall, the micrometer-sized NiOOH hierarchical sphere can be an attractive candidate as heterogeneous catalyst for PMS activation. This study provides a novel strategy *via* synergistic adsorption and catalytic oxidation for SR-AOPs system in water treatment.

Declaration of competing interests

The authors declare that they have no known competing financial interests or personal relationships that could have appeared to influence the work reported in this paper.

Acknowledgments

The present work was funded by the National Key R&D Program of China (No. 2018YFC0406503), the National Natural Science Foundation of China (No. 52070086), the Natural Science Foundation of Jilin Provincial Science & Technology Department (No. 20200403034SF) and the Open Project Program of Engineering Research Center of Groundwater Pollution Control and Remediation, Ministry of Education.

Supplementary materials

Supplementary material associated with this article can be found, in the online version, at doi:10.1016/j.cclet.2021.07.012.

References

[1] F. Hayati, A.A. Isari, B. Anvaripour, M. Fattahi, B. Kakavandi, Chem. Eng. J. 381 (2020) 122636.
[2] Y. Yang, L. Xu, W. Li, et al., Appl. Catal. B 259 (2019) 118057.
[3] C. Tan, X. Lu, X. Cui, et al., Chem. Eng. J. 363 (2019) 318–328.
[4] C. Tan, X. Jian, Y. Dong, et al., Chem. Eng. J. 359 (2019) 594–603.
[5] S. Zhu, X. Li, J. Kang, X. Duan, S. Wang, Environ. Sci. Technol. 53 (2019) 307–315.
[6] G. Chen, X. Zhang, Y. Gao, et al., Sep. Purif. Technol. 213 (2019) 456–464.
[7] P. Duan, Y. Qi, S. Feng, et al., Appl. Catal. B 267 (2020) 118717.
[8] S. Yanan, X. Xing, Q. Yue, B. Gao, Y. Li, Environ. Sci.: Nano. 7 (2020) 1444–1453.
[9] C. Cui, L. Jin, L. Jiang, et al., Sci. Total Environ. 572 (2016) 244–251.
[10] Y. Liu, Y. Wang, Q. Wang, J. Pan, J. Zhang, Chemosphere 190 (2018) 431–441.
[11] M. Gągol, A. Przyjazny, G. Boczkaj, Chem. Eng. J. 338 (2018) 599–627.
[12] Y. Pang, H. Lei, Chem. Eng. J. 287 (2016) 585–592.
[13] C. Lyu, Y. Li, C. Fang, et al., Chem. Res. Chin. Univ. 35 (2019) 440–448.
[14] Z. Wang, Y. Du, Y. Liu, et al., RSC Adv. 6 (2016) 11040–11048.
[15] Y. Huang, B. Sheng, Z. Wang, et al., Water Res. 145 (2018) 453–463.
[16] J. Wang, S. Wang, Chem. Eng. J. 334 (2018) 1502–1517.
[17] J. Peng, C. Zhang, Y. Zhang, et al., Ecotoxicol. Environ. Saf. 198 (2020) 110676.
[18] Y. Dong, X. Cui, X. Lu, et al., Sci. Total Environ. 662 (2019) 490–500.
[19] J. Deng, C. Ya, Y. Ge, et al., RSC Adv. 8 (2018) 2338–2349.
[20] L. Chen, H. Ji, J. Qi, et al., Chem. Eng. J. 406 (2021) 126877.
[21] M. Ma, L. Chen, J. Zhao, W. Liu, H. Ji, Chin. Chem. Lett. 30 (2019) 2191–2195.
[22] F. Pan, H. Ji, P. Du, et al., J. Hazard. Mater. 402 (2021) 123779.
[23] D. Yue, X. Qian, M. Ren, et al., Sci. Bull. 63 (2018) 278–281.
[24] D. Yue, C. Guo, X. Yan, et al., Chem. Eng. J. 360 (2019) 97–103.
[25] X. Qin, X. Li, L. Yang, et al., J. Alloys Compd. 610 (2014) 549–554.
[26] F. Gao, Y. Li, B. Xiang, Ecotoxicol. Environ. Saf. 158 (2018) 239–247.
[27] J. Brame, M. Long, Q. Li, P. Alvarez, Water Res. 60 (2014) 259–266.
[28] S. Saud, D.B. Nguyen, S.G. Kim, et al., Catalysts 10 (2020) 133–145.
[29] F. Li, Z. Wei, K. He, et al., Water Res. 185 (2020) 116219.
[30] C. Dang, F. Sun, H. Jiang, et al., J. Hazard. Mater. 400 (2020) 123225.
[31] C.G. Lee, H. Javed, D. Zhang, et al., Environ. Sci. Technol. 52 (2018) 4285–4293.
[32] Y. Nosaka, A.Y. Nosaka, Chem. Rev. 117 (2017) 11302–11336.
[33] C.W. Hu, Y. Yamada, K. Yoshimura, Sol. Energy Mater. Sol. Cells 177 (2018) 120–127.
[34] F. Ghanbari, M. Moradi, Chem. Eng. J. 310 (2017) 41–62.
[35] T. Chen, Q. Hao, W. Yang, et al., Appl. Catal. B 237 (2018) 442–448.
[36] M. Jayalakshmi, M.M. Rao, K.B. Kim, Int. J. Electrochem. Sci. 1 (2006) 324–333.
[37] T. Kundu, J. Wang, Y. Cheng, et al., Dalton Trans. 47 (2018) 13824–13829.
[38] E. Shangguan, H. Tang, Z. Chang, X.Z. Yuan, H. Wang, Int. J. Hydrog. Energy 36 (2011) 10057–10064.
[39] X.Z. Fu, X. Wang, Q.C. Xu, et al., Electrochim. Acta 52 (2007) 2109–2115.
[40] P.M. Carraro, T.B. Benzaquén, M.I. Oliva, G.A. Eimer, Chem. Phys. Lett. 713 (2018) 91–97.
[41] C. Li, X. Zhu, H. He, et al., J. Mol. Liq. 274 (2019) 353–361.
[42] J.C. Serna-Carrizales, V.H. Collins-Martínez, E. Flórez, et al., J. Mol. Liq. 324 (2021) 114740.
[43] Y. Liu, Y. Peng, B. An, L. Li, Y. Liu, Chemosphere 246 (2020) 125778.
[44] H. Liang, J. Lin, H. Jia, et al., J. Power Sources 378 (2018) 248–254.
[45] Q. Zhang, D. He, X. Li, et al., J. Hazard. Mater. 384 (2020) 121350.
[46] X. Duan, C. Su, L. Zhou, et al., Appl. Catal. B 194 (2016) 7–15.
[47] P. Shao, J. Tian, F. Yang, et al., Adv. Funct. Mater. 28 (2018) 1705295.
[48] P. Pieta, A. Petr, W. Kutner, L. Dunsch, Electrochim. Acta 53 (2008) 3412–3415.
[49] Z.S. Zhu, X.J. Yu, J. Qu, et al., Appl. Catal. B 261 (2020) 118238.
[50] J. Chauvin, F. Judee, M. Yousfi, P. Vicendo, N. Merbahi, Sci. Rep. 7 (2017) 4562–4576.
[51] H. Zhang, C. Zhou, H. Zeng, L. Deng, Z. Shi, J. Hazard. Mater. 395 (2020) 122613.
[52] J. Sun, Q. Wang, J. Zhang, Z. Wang, Z. Wu, Electrochim. Acta 277 (2018) 77–87.
[53] J. Lu, T. Wang, Y. Zhou, et al., J. Hazard. Mater. 383 (2020) 121133.